Desiccation cracks in dispersion of ellipsoids: Effect of aspect ratio and applied fields

Hisay Lama,[1,2] Madivala G. Basavaraj,[2] and Dillip K. Satapathy[1,*]
[1]*Soft Materials Laboratory, Department of Physics, Indian Institute of Technology Madras, Chennai 600036, India*
[2]*PE and CS Laboratory, Indian Institute of Technology Madras, Chennai 600036, India*

(Received 26 February 2018; revised manuscript received 5 July 2018; published 13 August 2018)

Particulate films obtained by drying colloidal dispersions often displaying a network of cracks are ubiquitous. In particulate films, drying-induced internal stresses are accumulated as a result of the consolidation of particles during solvent evaporation and are released by the formation of cracks. The morphology of crack patterns can be controlled by externally applied fields, modulation of drying kinetics, or by exploiting the shape anisotropy of the colloids. Here, we explore the role of particle shape anisotropy and externally applied thermal and magnetic fields on the evolution of cracks by performing desiccation experiments, i.e., by drying colloidal-ellipsoid-laden sessile drops on solid substrates. We determine the critical aspect ratio (α_c), where the cracks in the dried particulate deposit drastically change their orientation from a radial to circular pattern. It is observed that the drying of drops consisting of ellipsoids at an elevated temperature enhances the randomness in the particle arrangement and brings nontrivial modifications to the crack pattern. In addition, we show that the randomness in the particle arrangement due to the thermal field can be compensated by the application of an external magnetic field and the orientation of cracks can be completely restored.

DOI: 10.1103/PhysRevMaterials.2.085602

I. INTRODUCTION

Drying a dispersion consisting of colloidal particles leads to the formation of a particulate film [1]. The controlled assembly of particles in these particulate deposits has been widely studied and can be controlled by tuning a number of parameters including drying conditions, particle concentration, colloidal interactions, particle shape, external field, or by using other additives. The structural defects such as cracks [2,3], delamination [4,5], and buckling [6,7] are very common features of such particulate films. Among these defects, the investigation of crack patterns has received a great deal of attention in recent times [2]. During dessication, internal stresses are generated within the film due to competition between the evaporation-induced shrinkage of the layer and its adhesion to the substrate which resists such shrinkage. When the stresses in the film reach a critical value, the accumulated stress energy creates new surfaces which is manifested in the form of cracks. In other words, these cracks arise due to the release of stress energy which is accumulated in the particulate film during the drying process [2,8]. The critical stress can be estimated by invoking the Griffith condition [9,10], i.e., by equating the stress energy released during cracking to the surface energy associated with the newly formed surface.

The crack morphology depends on the drying condition, drying geometry, shape of the particles, constituents of drying suspension, etc. [1,6,11,13–15]. Various kinds of crack morphologies such as wavy, starlike, linear, circular, spiral, radial [1], and hierarchical [11] have been reported. In addition, very often they also exhibit a high degree of spatial periodicity [12,13]. Interestingly, both periodic and random cracks are useful in various technological applications [2,16,17] such as fabrication of lithographic templates. Externally applied electric, magnetic, or thermal fields can also be exploited to control the crack morphology in particulate film [18–23]. Thus, there is growing interest in the development of strategies for the rational design of crack patterns [17].

The particle shape has been identified as an important parameter that affects various colloidal scale phenomena including coffee-ring formation, emulsion stabilization, and self-assembly [24]. In particular, for elongated particles such as ellipsoids, the aspect ratio can affect the packing density of the particles, the coordination number, as well as the mechanical integrity of the particulate film [25,26]. Recently, we reported that the particulate films formed after complete drying of colloidal dispersion consisting of spherical particles exhibit radial cracks, whereas elliptical particles of aspect ratio $\alpha > 2.4$ form circular cracks [27]. However, the existence of a critical aspect ratio α_c, if any, where the transition from radial to circular cracks occurs, is not known. The effect of a thermal field provided via substrate heating facilitates the formation of a particulate film with quasiperiodic cracks in the dessication of spherical particles [28]. However, the influence of the thermal field on crack morphology formed in particulate deposits consisting of shape-anisotropic particles remains unexplored. In addition, the interplay between external fields such as magnetic and thermal fields and its role in crack formation also remain unknown. The possibility of using multiple external fields may provide an additional handle to control the self-assembly of particles and will facilitate the development of novel methodologies to control crack morphology.

In this work, by drying sessile drops containing model colloidal ellipsoids in the presence of magnetic and thermal fields, we have investigated the effect of external fields on

*dks@iitm.ac.in

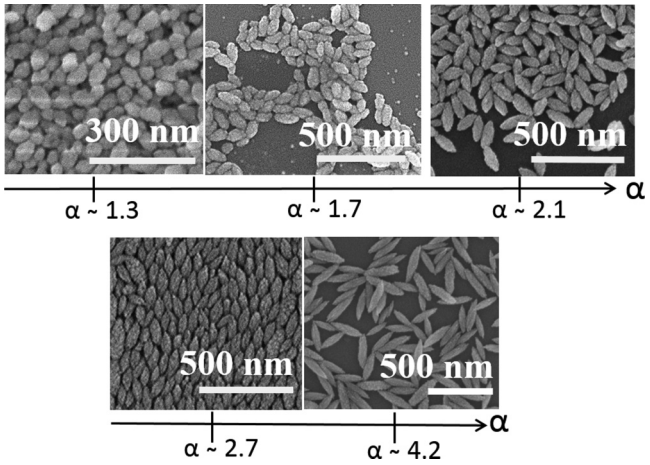

FIG. 1. Top to bottom: The scanning electron microscopy images of the hematite particles with aspect ratio α varying from ~1.3 to 4.2.

the crack pattern. Colloidal dispersions consisting of hematite ellipsoids of aspect ratio α varying from 1 to 4.0 were used to explore the effect of particle shape anisotropy. In particular, we report on (i) the effect of particle shape anisotropy on the crack morphology, wherein we estimate the critical aspect ratio α_c across which the particulate films display different crack patterns; (ii) influence of the thermal field on the crack pattern for α varying from 1 to 4.0; (iii) the effect of the interplay between thermal and magnetic fields on the self-assembly of ellipsoids in the particulate deposit and the resulting crack patterns. We show that the particulate deposits of ellipsoids of aspect ratios from 1 to 4.0 display different crack patterns, namely radial, circular, or their combination. At a critical aspect ratio, $\alpha_c \approx 1.7$, the particulate film begins to exhibit circular cracks instead of the usual radial cracks. The effect of thermal field on crack morphology is studied by tuning the substrate temperature T_{sub}. With an increase in substrate temperature, the particulate films with shape-anisotropic particles exhibit cracks with diminishing spatial periodicity accompanied by the change in the orientation of particles. The ellipsoids in the deposit that show positional and orientational order at $T_{sub} = 25\,^{\circ}$C become progressively disordered with increasing substrate temperature. However, we show that the orientation of ellipsoids and their long-range self-assembly dictate the crack morphology; the crack ordering can be restored by the application of an external dc magnetic field.

II. MATERIALS AND METHODS

A. Synthesis and characterization of hematite ellipsoids

The hematite particles (alpha-Fe_2O_3) with aspect ratio α varying from 1.3 to 4.2 (see Fig. 1) used in drying experiments were synthesized by the force hydrolysis method [29,30]. More details of the synthesis procedure can be found in the Supplemental Material [31]. The average size and the aspect ratio of the particles were estimated from high-resolution scanning electron microscopy (Hitachi S-4800, Japan) images using ImageJ software. The details of the particle dimensions are tabulated in Table I. The crystal structure of hematite ellipsoids

TABLE I. The size of the hematite ellipsoids.

Length, L (nm)	Diameter, d (nm)	$\alpha = L/d$
57 ± 8	42 ± 6	1.3 ± 0.2
100 ± 10	53 ± 4	1.7 ± 0.2
130 ± 21	61 ± 7	2.1 ± 0.3
140 ± 10	52 ± 3	2.7 ± 0.4
243 ± 12	56 ± 2	4.2 ± 0.2

is confirmed by performing x-ray diffraction experiment by using a SmartLab-Rigaku x-ray diffractometer. The peaks in the measured intensity versus diffraction angle plot are found to match with literature reports [32]. The magnetic properties of hematite ellipsoids are studied by performing the magnetization versus magnetic field intensity study using an MPMS SQUID magnetometer. The particles show hysteresis behavior with a very low coercive field (~80 G to 180 G) indicating that the particles are antiferromagnetic in nature. In addition, polystyrene (PS) beads of diameter 60 ± 8 nm, functionalized with the amidine group, are also used. They were purchased from Invitrogen (Oregon, USA) and supplied with a concentration of 4.1% wt/v. The surface charge density of the PS spheres is 4.8 μC/cm^2 (as per manufacturer). The concentration of the particle dispersion was adjusted by diluting the stock dispersion with Milli-Q water (resistivity ~18.2 MΩ cm).

B. Sessile drop evaporation

Drying experiments were carried out by placing sessile drops on glass substrates kept on top of a thermoelectric Peltier module (TEC 12706 with power rating 12 V, 92.4 watts) which is placed between the pole of pieces of an electromagnet separated by ~2.5 cm as shown in Fig. 2. The temperature of the Peltier stage can be varied from 25 °C to 60 °C by varying the current flowing through the Peltier. The temperature of the substrate T_{sub} is monitored using a thermocouple (K-type thermocouple purchased from MASTECH). The microscopy glass slides were used as substrates in all the drying experiments. These substrates were first cleaned using piranha solution consisting of H_2SO_4 and H_2O_2 in 3:1 ratio, then they were washed with Milli-Q water, acetone, and finally dried with dry N_2 gas. In all the experiments, 2 μL aqueous dispersion of hematite ellipsoids is used. The concentration of particles in the dispersion is $\phi \sim 3.0$ wt %. The pH of the initial dispersion is adjusted to 2 by adding an appropriate quantity of HNO_3. At this pH the hematite particles are positively charged, which is required for obtaining a coffee-ring-like deposit after sessile drop evaporation [30]. All the experiments are performed at a relative humidity RH $= 35 \pm 5\%$ and the temperature of the surrounding environment was maintained at $T_{amb} = 25 \pm 3\,^{\circ}$C. The following experiments were carried out: (1) evaporation of sessile drops containing ellipsoids of different aspect ratios at $T_{sub} = 25\,^{\circ}$C, (2) evaporation of sessile drops of ellipsoids of different aspect ratios on heated substrates ($T_{sub} = 25\,^{\circ}$C to $T_{sub} = 60\,^{\circ}$C), and (3) evaporation of sessile drops containing ellipsoids of aspect ratio 4 from $T_{sub} = 25\,^{\circ}$C to $T_{sub} = 60\,^{\circ}$C under the application of an external magnetic field. For case (3), at each T_{sub}, the magnetic field is varied from 5 G to 100 G.

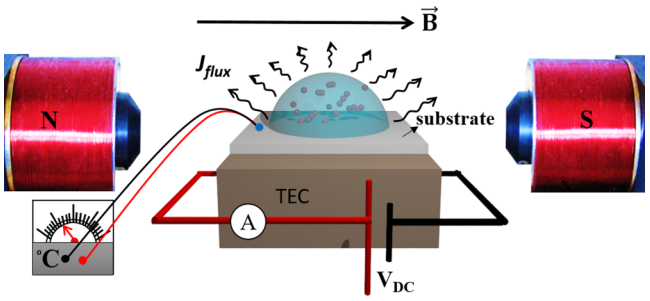

FIG. 2. Schematic of the experimental setup showing a sessile droplet of colloidal suspension placed on a substrate kept on the thermoelectric heating module (TEC). The sessile drop is placed between the poles of the electromagnet separated by a distance of ∼2.5 cm. The north pole and south pole of the electromagnet are marked. The arrows around the drop surface indicate the inhomogeneous evaporative flux J_{flux}, and the horizontal arrow depicts the direction of the applied magnetic field. The thermocouple attached to the multimeter used for measuring the temperature of the substrate is also shown in the schematic.

The deposit pattern obtained after complete drying under various experimental conditions is observed under an optical microscope (Leica DMI1300B, Germany). The microstructure of the deposit and the particles is observed with a high-resolution scanning electron microscope (HRSEM, Hitachi S-4800, Japan). The thickness of the deposit is monitored using an optical surface profile meter (Bruker, Contour GT-1, Germany).

III. RESULTS AND DISCUSSION

A. Effect of aspect ratio of ellipsoids on morphology of desiccation cracks

The bright-field optical microscopy images of a section of dried deposit obtained by evaporation of sessile drops containing ellipsoids of different aspect ratios $\alpha \sim 1.3$–4.2 are shown in Fig. 3. These deposits were obtained as a result of drying a 2 μL drop of 3.0 wt % colloidal suspension at $T_{\text{amb}} \approx 25\,^{\circ}\text{C}$ and in the absence of external field. The particulate deposit consisting of ellipsoids of the lowest aspect ratio studied, $\alpha \sim 1.3$, exhibits radial cracks as shown in Fig. 3(a). When the aspect ratio of the particles in the sessile drop is increased to $\alpha \sim 1.7$, the dried deposit exhibits radial cracks along with circular cracks at the outer edge as shown in Fig. 3(b). Upon slightly increasing the particle aspect ratio to $\alpha \sim 2.1$, the deposit pattern is dominated solely by circular cracks as shown in Figs. 3(c)–3(e). However, there is no significant variation in the width w of the deposit with different aspect ratios as evident from Fig. 3. The average width of the dried deposit is around 140 ± 8 μm. The schematic and SEM images shown in Figs. 4(a)–4(c) and Figs. 4(d)–4(f), respectively, highlight the correlation between different crack morphologies and the aspect ratio of particles. The SEM image shown in Fig. 4(d) displays the arrangement of ellipsoids with $\alpha \approx 1.3$ in the particulate film at the vicinity of the cracks. The particles are closely packed and the deposit is structurally isotropic (i.e., the orientation effect is least significant) since they are nearly spherical. The isotropic arrangement of particles is also confirmed from the fast Fourier transform (FFT) pattern performed on the surface of the deposit and is shown in Fig. 4(g). In the particulate films with ellipsoids of $\alpha \sim 1.7$ and higher, an ordered alignment of ellipsoids is observed in the vicinity of the cracks as shown in Fig. 4(e). However, in regions away from the cracks, domains of a randomly arranged particle assembly are observed as marked by a red box in Fig. 4(e). The FFT pattern shown in Fig. 4(h) shows the slight deviation from the nearly isotropic pattern. The deposit pattern consisting of particles with $\alpha > 2.1$ shows circular cracks with the particles being aligned such that their major axis lies parallel to the crack path as shown in Fig. 4(f). The FFT pattern for these deposits indicates a high degree of anisotropy as shown Fig. 4(i), which clearly reveals the emergence of the orientation of particles along a preferred direction. Unlike the previous case, here the highly ordered particle arrangement persists farther away from the cracks. Interestingly, for our experimental system, the crack patterns recorded at elevated temperatures also show a very similar transition from radial to circular cracks and it again occurs at a narrow aspect ratio range

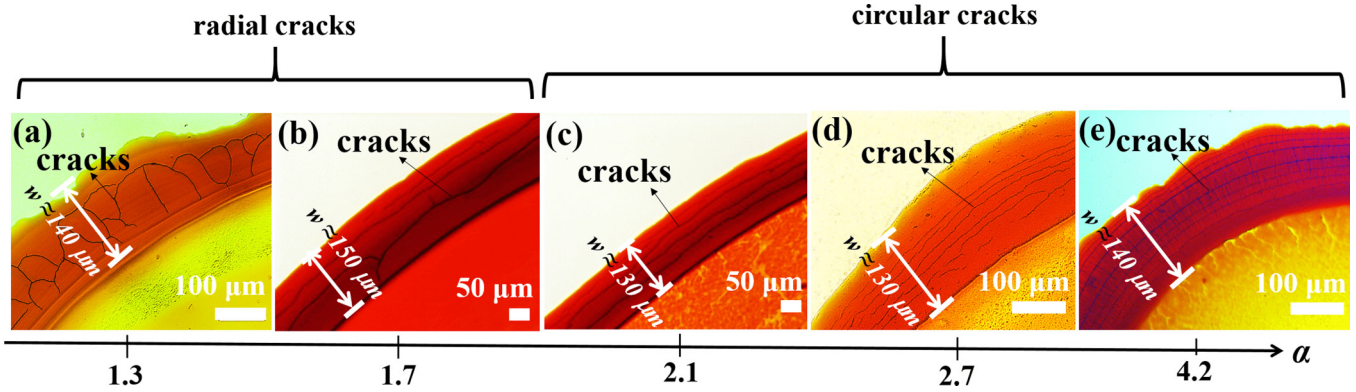

FIG. 3. Optical microscopy images show the crack morphology in the deposit of ellipsoids having various aspect ratios $\alpha \sim 1.3$ to 4.2. (a) Network of cracks in the annular region of width w oriented predominantly along the radial direction in the deposit for ellipsoids of $\alpha \approx 1.3$. (b) Combination of radial and circular cracks in the deposit for ellipsoids of $\alpha \approx 1.7$. (c), (d), and (e): Circular cracks in the deposit for ellipsoidal particles with $\alpha \approx 2.1$, 2.7, and 4.2, respectively. The widths w of the deposit are marked in the respective microscopy images.

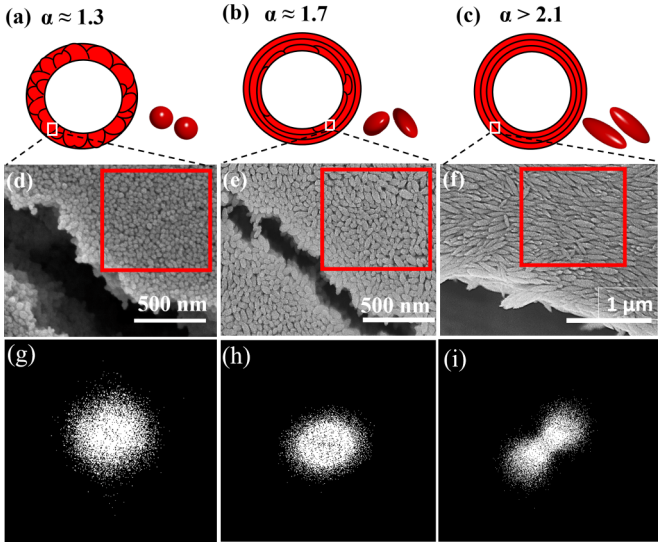

FIG. 4. Schematic of the dried particulate deposit for (a) $\alpha \approx 1.0$, (b) $\alpha \approx 1.7$, and (c) $\alpha > 2.1$. SEM micrographs depict the particle assembly in the vicinity of the cracks for the deposits with particle aspect ratio (d) $\alpha \approx 1.0$, (e) $\alpha \approx 1.7$, and (f) $\alpha > 2.1$. (g)–(i): The fast Fourier transform (FFT) pattern of the deposit surface enclosed by the rectangular marked region in the respective SEM micrographs. A clear evolution from the nearly isotropic to anisotropic FFT pattern is observed corresponding to a transition in the crack morphology from radial to circular.

(1.8–2.7) irrespective of the substrate temperature as shown in Fig. S1 of the Supplemental Material [31]. This suggests that at least for the hematite ellipsoids, the critical aspect ratio for the morphological transition from radial to circular cracks remains invariant under varying fluid evaporation rate. The universality of the aspect-ratio-dependent radial-to-circular transition can be established by doing further experiments using other types of ellipsoids of tunable aspect ratio, e.g., silica and polystyrene, and tuning experimental parameters such as substrate wettability, rate of evaporation, particle concentration, colloidal interaction, and fluid viscosity over a wide range.

Now we turn to explain the observed transition in the crack morphology with particle aspect ratio by studying the variation in the microstructure of the dried deposits. The evaporation of sessile drops containing spherical/nonspherical particles under the aforementioned conditions leads to the accumulation of the particles at the periphery of the drying drop [27,33]. The stress σ generated at the surface of the semidried region in the deposit where the particles are accumulated is determined by the local liquid pressure p in the voids (or interstitial spaces) of the particulate film. The σ at any instant t on the surface of the deposit can be expressed as [14]

$$\sigma(h(r), t) \approx p_0 - p(h(r), t), \tag{1}$$

where $h(r)$ is the instantaneous height of the deposit at a distance r from the center of the drop and p_0 is the constant hydrostatic pressure exerted on the pores in the initial semidried gel phase of the particulate deposit. This hydrostatic pressure p_0 is equivalent to the atmospheric pressure, i.e., $p_0 = p_{\text{atm}} \approx 10^5$ N/m^2. The local pressure $p(h(r), t)$ increases with time as the fluid continues to evaporate. Now if we consider the semidried deposit as a porous-elastic film with Young's modulus E through which the fluid evaporates at the rate v_E, the height-averaged stress generated in the film due to drying can be obtained from the poroelastic model [14,34]:

$$\overline{\sigma(h(r), t)} \approx \frac{t\, v_E E}{h(r)}. \tag{2}$$

The detailed derivation can be found in the Supplemental Material [31]. Note that the stress $\bar{\sigma}$ increases linearly with time as fluid evaporates from the particulate deposit. Since the cracks nucleate at the very end of drying, i.e., when the particles in the deposit are almost in contact, the void radius is the least and $p(h(r), t) \approx P_{\text{cap}}$. P_{cap} is the capillary pressure and is expressed as $P_{\text{cap}} = g\gamma/r$, where g is the geometric factor (depends on the shape of fluid meniscus), γ is the surface tension of the suspension, and r is the void radius [14]. The magnitude of P_{cap} is estimated to be about 10^7 N/m^2 which clearly implies $P_{\text{cap}} \gg p_0$. The stress accumulated in the particulate film reaches its maximum value towards the tail end of the solvent evaporation. Interestingly, the cracks in the particulate deposit also appear at the final stage of the drying when the built-up stress in the particulate deposit exceeds the critical value σ_c. This suggest that σ_c is nearly equal to P_{cap}. Thus, at the onset of crack formation, $\overline{\sigma(h(r), t)} = \sigma_c \approx -P_{\text{cap}}$. The critical stress and P_{cap} are both inversely proportional to the void radius [35].

The voids in the particulate film usually act as defect sites at which the drying stress concentrates as its radius decreases upon evaporation of the fluid. When the drying stress increases to a critical value σ_c, the cracks nucleate at the vicinity of voids. Further, the crack propagation is favored when the energy released per unit crack length G during the crack formation is greater than or equal to the work done in creating two new surfaces, i.e., $G \geqslant G_c$, where G_c is the critical energy release rate [9]. Moreover, it is known that the crack in the colloidal films propagates through the least resistant path [27]. From the SEM images shown in Figs. 4(d)–4(f), it is evident that the cracking on surface of the deposit results in the physical separation of particles. The particles in the vicinity of the cracks are found to be closely packed and the degree of ordering of particles increases with increase in α. The particulate deposit with particles of $\alpha \approx 1.3$ is structurally isotropic as shown in Fig. 4(a), and the crack morphology mostly depends on the radial fluid flow. Since there is no preferential least-resistant path for the cracks to propagate, the cracks are radial. However, structural anisotropy in the particulate deposit can be induced with an increase in aspect ratio as shown in Figs. 4(e) and 4(f). The structural anisotropy of the deposit gets enhanced with increase in α due to the shape-induced preferential orientation of ellipsoids which further dictates the crack path and leads to the formation of concentric circular cracks. The nondimensional parameters such as the Reynolds number Re, capillary number Ca, Peclet number Pe, and Marangoni number Ma relating the relative influence of fluid flows during the drying process were also estimated and are shown in Table S1 of the Supplemental Material [31]. For our experimental system, these numbers do not vary significantly with an increase in the aspect ratio of the particles.

B. Effect of thermal field on crack morphology

After discussing the effect of particle shape on the morphology of cracks, we now turn to discuss the effect of thermal field on particle arrangement and crack morphology. The experimental system is similar except that the sessile drop containing colloids is now placed on a preheated substrate maintained at a constant temperature (T_{sub}). T_{sub} is changed from 25 to 50 °C leading to the variation in thermal energy, $k_B T_{sub}$, between 4.1 and 4.5×10^{-21} J (where k_B is the Boltzmann constant $= 1.38 \times 10^{-23}$ J K^{-1}).

Anisotropic particles ($\alpha \approx 4.2$). The effect of substrate temperature on the crack pattern formed on the dried particulate deposits consisting of shape-anisotropic particles with $\alpha \approx 4.2$ is shown in Fig. 5. As can be seen from the figure, cracks are formed in the annular region of the deposit of width w (marked in the figure). The periodic circular cracks are observed for $T_{sub} \approx 25$ °C and 34 °C as seen in Figs. 5(a) and 5(c). The ellipsoids in the vicinity of the cracks on the surface of the deposit exhibit a high degree of ordering and orient with their major axis parallel to the cracks as evident from SEM image shown in Figs. 5(b) and 5(d). A similar arrangement, with the major axis parallel to the crack direction, also persists throughout the crack surfaces created to release the internal stresses as shown in the encircled region in Fig. 5(d). On the other hand, the deposits obtained at $T_{sub} \approx 40$ °C also exhibit circular cracks which are discontinuous and nonperiodic as shown in Fig. 5(e). The orientation of ellipsoids in the vicinity of the cracks on the deposit surface is not as prominent as compared to that obtained at $T_{sub} \approx 25$ °C and at 34 °C. At $T_{sub} \approx 50$ °C fragmented tiny cracks are observed as shown in Fig. 5(g). The arrangement of ellipsoids on the deposit surface at this temperature is completely random as can be seen from Fig. 5(h). However, along the cross section of the deposit, i.e., on the pair of surfaces newly created by the cracks, the parallel alignment of ellipsoids still persists and it is shown in the region marked by the dashed line in Fig. 5(h). The FFTs of the SEM image (marked rectangular region) shown in the insets of Figs. 5(b) and 5(h) depict that a nematic to isotropic transition in the particle arrangement occurs on the surface of the dried deposit with the increase in T_{sub}. It must be noted that the overall nature of cracks remains circular (not radial) for $T_{sub} \approx 40$ °C and 50 °C, albeit given the isotropic nature of the particle arrangement on the surface of the deposit. This suggests that the arrangement of particles in the bulk largely dictates the overall crack morphology.

Now we turn to explain the observed evolution of crack morphology from concentric circular cracks at low T_{sub} to fragmented cracks with increase in T_{sub}. The evaporation of a sessile drop of nonspherical colloids typically leads to deposition of the particles towards the edge of the drop, and the particles align with their major axis parallel to the droplet periphery [27,30]. The alignment of the particles arises due to the hydrodynamic torque experienced by the particles at the droplet periphery during the process of evaporation [23]. With the increase in T_{sub}, there is an increase in thermal energy $k_B T_{sub}$ of the particles and a decrease in the time required for the complete evaporation of the sessile drop t_f. By increasing the substrate temperature from $T_{sub} \approx 25$ °C to 50 °C, the thermal energy increases from 4.1 to 4.5×10^{-21} J

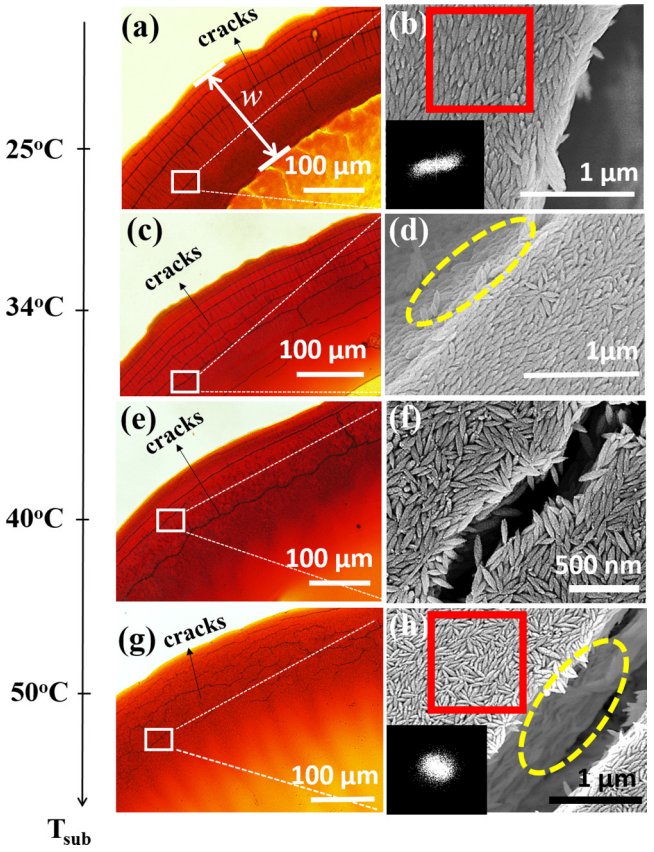

FIG. 5. Optical microscopy images of the section of the dried particle deposit ($\alpha \approx 4.2$) depict (a) deposit with circular cracks at $T_{sub} \approx 25$ °C, (c) circular crack with wider ring width w at $T_{sub} \approx 34$ °C, (e) zigzag cracks on the deposit at $T_{sub} \approx 40$ °C, and (g) fragmented shorter cracks at $T_{sub} \approx 50$ °C. The SEM images depict the region inside the rectangular box marked in the microscopy image for corresponding temperatures. (b) Close-packed assembly of the ellipsoids in the vicinity of the cracks at $T_{sub} \approx 25$ °C; (d) close-packed assembly in the vicinity of the cracks at $T_{sub} \approx 34$ °C. (f) At $T_{sub} \approx 40$ °C the SEM micrograph depicts the random orientation of the particle. (h) Ellipsoids on the surface of the deposit are completely randomly arranged at $T_{sub} \approx 50$ °C. The FFT was performed on the surface of the particulate deposit for a region enclosed by the rectangles in the SEM micrographs and that are shown in the insets of (b) and (h). The width w of the deposit is also marked. The vertical cross section showing the parallel alignment of ellipsoids along the crack is shown in an encircled region (also given in Fig. S2 of the Supplemental Material [31]).

while the t_f decreases from 480 to 100 seconds. The increase in thermal energy brings randomness into the system which possibly facilitates the random arrangement of the particles on the surface of the deposit. Another reason for the observed disorderedness could be the interfacial capture of the ellipsoids by the rapidly descending interface at high T_{sub}. Thus, particles captured by the interface are deprived of the time required to form an ordered arrangement due to the presence of strongly shape-induced capillary interaction [36], whereas particles in the bulk of the deposit are largely unaffected by this phenomena and the ordered arrangement is preserved as shown in Fig. 5(h). An increase in T_{sub} enhances the temperature gradient between

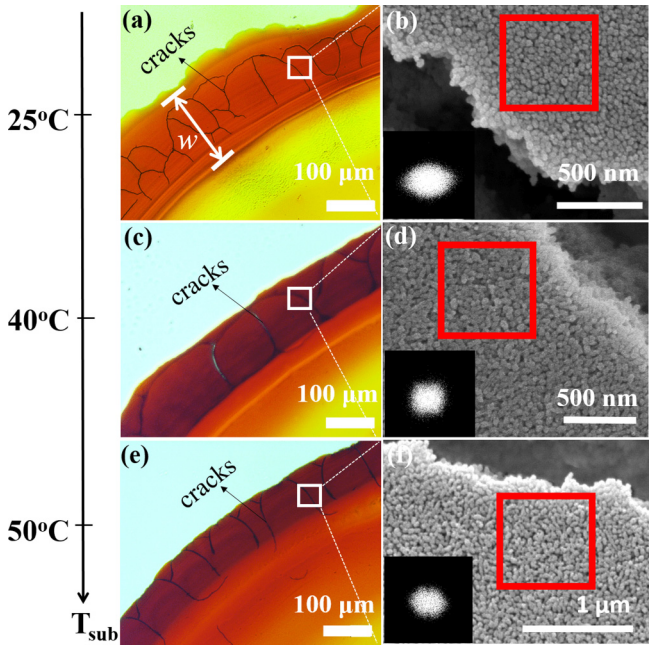

FIG. 6. Optical microscopy images of the section of the dried particle deposit ($\alpha \approx 1.3$) at (a) $T_{sub} \approx 25\,^{\circ}$C, (c) 40 °C, and (d) 50 °C. The corresponding SEM images showing the particle arrangement in the vicinity of the cracks and in the rectangular box regions marked are at (b) $T_{sub} \approx 25\,^{\circ}$C, (d) 40 °C, and (f) 50 °C. The FFT patterns depicting the arrangement of the particles on the surface of the particulate deposit for the regions enclosed by the rectangles in the SEM micrographs are shown in the respective insets. The width w of the deposit is also marked.

the drop apex and its edge which facilitates the Marangoni flow. This leads to a coffee-ring-like deposit with larger width w and sometime the central stain [28].

Nearly isotropic particles ($1.0 \leqslant \alpha \leqslant 1.3$). We further investigate the effect of T_{sub} on the crack pattern formed on the particulate deposits consisting of nearly spherical hematite particles, i.e., with $1.0 \leqslant \alpha \approx 1.3$. Sessile drops containing low-aspect-ratio ellipsoids ($\alpha \sim 1.3$) were evaporated under similar conditions and the formation of ringlike particulate deposits with cracks was observed. The optical microscopy images of the region of the ring exhibiting cracks for the suspension evaporated at $T_{sub} \approx 25\,^{\circ}$C, 40 °C, and 50 °C are shown in Figs. 6(a), 6(c), and 6(e), respectively. The cracks in the deposit formed at $T_{sub} \approx 25\,^{\circ}$C are nearly random and form an interconnected network as can be seen in Fig. 6(a). The number density of cracks (i.e., number of cracks per unit perimeter length) seems to be higher for droplets evaporated at lower substrate temperatures. The corresponding SEM image recorded at the vicinity of the cracks reveals that the particles are closely packed with a nearly isotropic arrangement with some preferential orientation as can be seen from FFTs shown in the inset of Fig. 6(b). The deposits obtained at higher substrate temperature, i.e., at $T_{sub} \approx 40\,^{\circ}$C and 50 °C, exhibit radial cracks. The microstructure of the deposit shows complete loss of the slight preferential ordering observed at low T_{sub} as evident in the SEM images and their FFTs shown in the insets of Figs. 6(d) and 6(f). Interestingly, despite the loss in ordering of particles an improvement in the ordering is observed for the cracks.

In order to verify the robustness of our findings showing the enhancement in the ordering of cracks with increase in T_{sub}, we repeated the experiments with another type of model spherical colloid. Sessile drops containing polystyrene spheres ($\alpha \approx 1.0$) with diameter about 60 nm were evaporated at different T_{sub}. We found that the deposit obtained at $T_{sub} \approx 25\,^{\circ}$C exhibits a disordered interconnected network of cracks with higher density near the edge of the drop. Moreover, at $T_{sub} \approx 40\,^{\circ}$C and 50 °C highly ordered radial cracks almost parallel to each other are observed. Further details and microscopy images are provided in Sec. V of the Supplemental Material [31]. The droplet evaporation phenomena and the mechanism of formation of ringlike particulate deposits at various T_{sub} values are similar for both the isotropic and anisotropic particles. However, at elevated temperatures, i.e., at $T_{sub} \geqslant 40\,^{\circ}$C, the crack patterns formed for shape-anisotropic particles and for shape-isotropic particles are opposite in nature. For shape-isotropic particles, a net enhancement in the ordering of cracks is observed whereas an antagonistic phenomenon, i.e., progressive disorderedness (smaller fragmented cracks), of the cracks is observed for shape-anisotropic particles with the increase in T_{sub}.

C. Combined effect of thermal and external magnetic field on crack morphology

In the previous section, we found that at $T_{sub} \approx 25\,^{\circ}$C the deposit consisting of shape-anisotropic particles exhibits circular cracks which becomes progressively disordered with the increase in T_{sub}. At $T_{sub} > 40\,^{\circ}$C, fragmented shorter cracks were observed. The effect was attributed to the evolution in the microstructure of the particle deposits with increase in T_{sub}. In this section, we show that the thermal-field-induced distortion in cracks can be suppressed and the ordering of cracks can be restored by the application of another external field, i.e., magnetic field. A sessile drop of shape-anisotropic-particle dispersion was placed on a preheated substrate maintained at a specific T_{sub} and was evaporated in the presence of an externally applied magnetic field $\vec{B}$. We have conducted these experiments by changing T_{sub} from 25 °C to 50 °C and with an external magnetic field varying from $|\vec{B}| = 5$ G to 100 G. The critical field, at which the particles align with their easy axis parallel to the magnetic field, is estimated to be ∼30 G [37]. The strength of the applied magnetic field during the process of drying is kept fixed at $|\vec{B}| = 50$ G; it is higher than that of the critical field. The optical microscopy images in Fig. 7 show part of the dried deposit and the crack morphology obtained by applying $|\vec{B}| = 50$ G and at $T_{sub} \approx 25\,^{\circ}$C, 40 °C, and 50 °C. The cracks were found to be perpendicular to the direction of the external applied magnetic field, which is indicated by an upward vertical arrow shown in Fig. 7. Spatially periodic cracks with a well-defined crack spacing λ are formed in marked contrast to those corresponding to the crack patterns formed in the absence of magnetic field shown in Figs. 5(e) and 5(g). The SEM images in Figs. 7(b), 7(d), and 7(f) reveal that the crack direction is again governed by the underlying microstructure wherein the ellipsoids are arranged with their

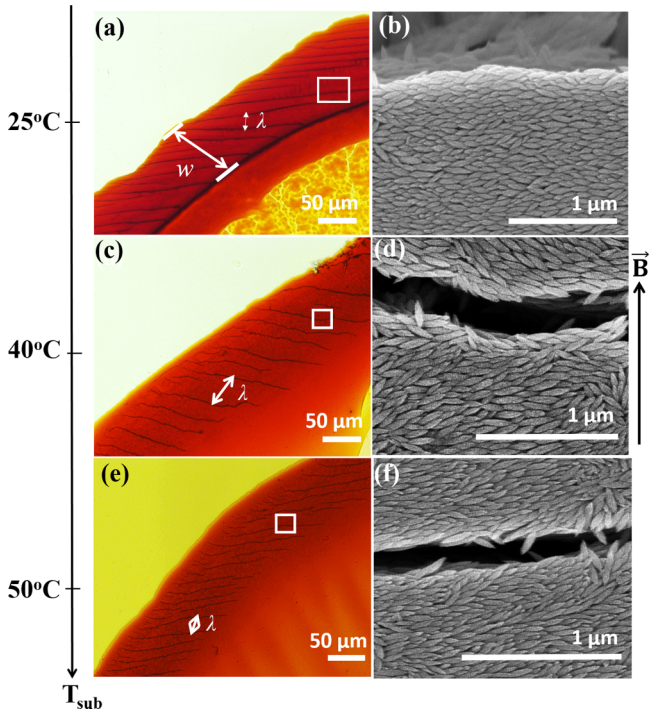

FIG. 7. Optical microscopy images of the section of the ringlike deposit with $\alpha \approx 4.0$ and $|\vec{B}| = 50$ G show the crack pattern at (a) $T_{sub} \approx 25\,^{\circ}$C, (c) $T_{sub} \approx 40\,^{\circ}$C, and (e) $T_{sub} \approx 50\,^{\circ}$C. SEM images of the rectangular regions marked in the microscopy images at (b) $T_{sub} \approx 25\,^{\circ}$C, (d) $T_{sub} \approx 40\,^{\circ}$C, and (f) $T_{sub} \approx 50\,^{\circ}$C show the respective microstructures. Width w and crack spacing λ are marked; the direction of magnetic field is indicated by an arrow.

major axis parallel to the crack direction irrespective of the substrate temperature.

Thus, the thermal field that tends to randomize the particle arrangement is overcome by the applied dc magnetic field. The enhanced ordering of particles at $T_{sub} \approx 50\,^{\circ}$C gives rise to ordered cracks. This provides an additional handle to manipulate the crack morphology by selectively tuning the magnitude of applied fields.

IV. CONCLUSION

To summarize, we presented a detailed study of the role of particle shape anisotropy and the external applied fields on the evolution of cracks by performing desiccation experiments. The coffee-ring-like deposits with spherical particles as well as particles of low aspect ratio ranging between $1.0 \leqslant \alpha < 1.3$ exhibit radial cracks while at aspect ratio $\alpha \geqslant 2.0$ circular cracks form. The critical aspect ratio at which the transition from radial to circular crack morphology occurs was found to be $\alpha_c \approx 1.7$. The transition in crack pattern from radial to circular is associated with the microstructural changes in the arrangement of particles in the deposits. The effect of the thermal field on the crack patterns in the particulate film consisting of shape-anisotropic particles is studied. For spherical particles, an improvement in the ordering of the cracks is observed. However, for ellipsoids of $\alpha > 2.0$, cracks become disordered with increase in T_{sub}. The periodicity in cracks is lowered with the increase in T_{sub} for ellipsoids ($\alpha > 2.0$) which is in stark contrast to spherical particles where the cracks become dramatically periodic with the increase in T_{sub}. Finally, we have studied the effect of interplay between the thermal and magnetic fields on the crack morphology. We found that the randomness in particle arrangement generated by the thermal energy can be completely suppressed by applying an external magnetic field. The alignment of particles with their easy axis parallel to the applied magnetic field leads to the formation of periodic cracks. Our experiments propose a modular approach to control the crack morphology in particle deposits obtained in desiccation experiments by a careful choice of particle aspect ratio and external fields.

ACKNOWLEDGMENTS

We thank Prof. N. Harish Kumar of the Department of Physics IIT Madras for providing us with a digital gaussmeter. We acknowledge the scanning electron microscopy facility of the Department of Physics IIT Madras. We also thank Megha Emerse, Soft Materials Laboratory IIT Madras, for assisting us in setting up the experimental system.

[1] A. F. Routh, Rep. Prog. Phys. **76**, 046603 (2013).
[2] L. Goehring, A. Nakahara, T. Dutta, S. Tarafdar, and S. Kitsunezaki, *Desiccation Cracks and Their Patterns: Formation and Modelling in Science and Nature* (Wiley-VCH, Weinheim, Germany, 2015).
[3] A. Groisman and E. Kaplan, Europhys. Lett. **25**, 415 (1994).
[4] V. Lazarus and L. Pauchard, Soft Matter **7**, 2552 (2011).
[5] F. Boulogne and H. A. Stone, Europhys. Lett. **108**, 19001 (2014).
[6] P. Xu, A. Mujumdar, and B. Yu, Drying Technol. **27**, 636 (2009).
[7] Y. Zhang, Y. Qian, Z. Liu, Z. Li, and D. Zang, Eur. Phys. J. E **37**, 1 (2014).
[8] W. P. Lee and A. F. Routh, Langmuir **20**, 9885 (2004).
[9] T. L. Anderson, *Fracture Mechanics: Fundamentals and Applications*, 3rd ed. (Taylor & Francis, New York, 2005).
[10] K. B. Singh and M. S. Tirumkudulu, Phys. Rev. Lett. **98**, 218302 (2007).
[11] S. Bohn, J. Platkiewicz, B. Andreotti, M. Adda-Bedia, and Y. Couder, Phys. Rev. E **71**, 046215 (2005).
[12] C. Allain and L. Limat, Phys. Rev. Lett. **74**, 2981 (1995).
[13] T. Ding, K. Song, K. Clays, and C.-H. Tung, Adv. Mater. **21**, 1936 (2009).
[14] F. Giorgiutti-Dauphiné and L. Pauchard, Eur. Phys. J. E **37**, 39 (2014).
[15] K. Piroird, V. Lazarus, G. Gauthier, A. Lesaine, D. Bonamy, and C. Rountree, Europhys. Lett. **113**, 38002 (2016).
[16] A. Kumar, R. Pujar, N. Gupta, S. Tarafdar, and G. U. Kulkarni, Appl. Phys. Lett. **111**, 013502 (2017).
[17] K. H. Nam, I. H. Park, and S. H. Ko, Nature (London) **485**, 221 (2012).
[18] M. Mittal and E. M. Furst, Adv. Funct. Mater. **19**, 3271 (2009).
[19] T. Khatun, M. D. Choudhury, T. Dutta, and S. Tarafdar, Phys. Rev. E **86**, 016114 (2012).

[20] L. Pauchard, F. Elias, P. Boltenhagen, A. Cebers, and J. C. Bacri, Phys. Rev. E **77**, 021402 (2008).
[21] J. Richardi, A. T. Ngo, and M. P. Pileni, J. Phys. Chem. C **114**, 17324 (2010).
[22] A. T. Ngo, J. Richardi, and M. P. Pileni, Nano Lett. **8**, 2485 (2008).
[23] H. Lama, V. R. Dugyala, M. G. Basavaraj, and D. K. Satapathy, Phys. Rev. E **94**, 012618 (2016).
[24] V. R. Dugyala, S. V. Daware, and M. G. Basavaraj, Soft Matter **9**, 6711 (2013).
[25] L. K. Roth and H. M. Jaeger, Soft Matter **12**, 1107 (2016).
[26] A. Donev, I. Cisse, D. Sachs, E. A. Variano, F. H. Stillinger, R. Connelly, S. Torquato, and P. M. Chaikin, Science **303**, 990 (2004).
[27] V. R. Dugyala, H. Lama, D. K. Satapathy, and M. G. Basavaraj, Sci. Rep. **6**, 30708 (2016).
[28] H. Lama, M. G. Basavaraj, and D. K. Satapathy, Soft Matter **13**, 5445 (2017).
[29] M. Ocaña, M. Morales, and C. Serna, J. Colloid Interface Sci. **212**, 317 (1999).
[30] V. R. Dugyala and M. G. Basavaraj, Langmuir **30**, 8680 (2014).
[31] See Supplemental Material at http://link.aps.org/supplemental/10.1103/PhysRevMaterials.2.085602 for optical and scanning electron microscopy images of cracks and the microstructure under different experimental conditions and details of hematite particle synthesis.
[32] L. Li, D. Qin, X. Yang, and G. Liu, Poly. Chem. **1**, 289 (2010).
[33] R. D. Deegan, O. Bakajin, T. F. Dupont, G. Huber, S. R. Nagel, and T. A. Witten, Nature (London) **389**, 827 (1997).
[34] M. A. Biot, J. Appl. Phys. **12**, 155 (1941).
[35] M. S. Tirumkudulu and W. B. Russel, Langmuir **21**, 4938 (2005).
[36] B. Madivala, J. Fransaer, and J. Vermant, Langmuir **25**, 2718 (2009).
[37] H. Lama, R. Mondal, M. G. Basavaraj, and D. K. Satapathy, J. Colloid Interface Sci. **510**, 172 (2018).